

**Broad  $K\alpha$  iron line from accretion disks around traversable wormholes**

Cosimo Bambi\*

*Center for Field Theory and Particle Physics and Department of Physics, Fudan University, 200433 Shanghai, China*

(Received 4 March 2013; published 15 April 2013)

It has been proposed that the supermassive black hole candidates at the centers of galaxies might be wormholes formed in the early Universe and connecting our Universe with other sister universes. The analysis of the profile of the relativistic  $K\alpha$  iron line is currently the only available approach to probe the spacetime geometry around these objects. In this paper, we compute the expected  $K\alpha$  iron line in some wormhole spacetimes and we compare the results with the line produced around Kerr black holes. The line produced in accretion disks around nonrotating or very slow-rotating wormholes is relatively similar to the one expected around Kerr black holes with mid or high value of spin parameter and current observations are still marginally compatible with the possibility that the supermassive black hole candidates in galactic nuclei are these objects. For wormholes with spin parameter  $a_* \geq 0.02$ , the associated  $K\alpha$  iron line is instead quite different from the one produced around Kerr black holes, and their existence may already be excluded.

DOI: [10.1103/PhysRevD.87.084039](https://doi.org/10.1103/PhysRevD.87.084039)

PACS numbers: 04.20.-q, 04.70.-s, 98.62.Js

**I. INTRODUCTION**

Nowadays, we have strong observational evidence that the center of every normal galaxy harbors a dark compact object with a mass  $M \sim 10^5\text{--}10^9 M_\odot$  [1]. While we believe that all these supermassive objects are the Kerr black holes (BHs) predicted by general relativity, their actual nature has still to be verified [2,3]. Dynamical measurements can provide robust estimates of the masses of these bodies. Combining these results with an upper bound for their radius, it turns out that these objects are too heavy, compact, and old to be clusters of nonluminous bodies [4]. The nonobservation of thermal radiation emitted by the putative surface of the BH candidate at the center of our Galaxy may also be interpreted as an indication that the latter has an event horizon and is therefore a BH [5] (see however Ref. [6]). Nevertheless, the exact origin of these objects is not clear: we do not understand how they could have become so heavy in such a short time, as we know BH candidates with a mass  $M \sim 10^9 M_\odot$  at redshift  $z \geq 6$  [7], i.e., just about 100 million years after the big bang.

A speculative possibility is that supermassive BH candidates are wormholes, topological connections between separated regions of the spacetime [8]. They may be relics of the early Universe and may connect either two different regions in our Universe or two different universes in a multiverse model. Such a scenario may also explain the nonobservation of thermal radiation, as wormholes do not have a surface. The possibility of the existence of wormholes cannot be ruled out by general arguments; it is not in contradiction with current observations, and the search for astrophysical wormholes could represent a unique opportunity to investigate a multielement Universe.

Some authors have already discussed possible ways to observationally distinguish a Kerr BH from a wormhole

[9,10]. However, previous work has never considered the analysis of the  $K\alpha$  iron line, which is currently the only available technique to probe the geometry of the spacetime around supermassive BH candidates [11].<sup>1</sup> The  $K\alpha$  iron line is intrinsically narrow in frequency, while the one observed appears broadened and skewed. The interpretation is that the line is strongly altered by special and general relativistic effects, which produce a characteristic profile first predicted in Ref. [15] and then observed for the first time in the ASCA data of the Seyfert 1 galaxy MCG-6-30-15 [16]. In this paper, we will use the code discussed in Refs. [13,17] to compute the profile of the  $K\alpha$  iron line produced around traversable wormholes and seen by a distant observer. We will then compare these lines with the ones produced from Kerr spacetimes, to check how this technique can test the wormhole nature of the supermassive BH candidates in galactic nuclei.

**II. PROFILE OF THE  $K\alpha$  IRON LINE**

The X-ray spectrum of both stellar-mass and supermassive BH candidates is usually characterized by the presence of a power-law component. This feature is commonly interpreted as the inverse Compton scattering of thermal photons by electrons in a hot corona above the accretion disk. The geometry of the corona is not known and several models have been proposed. Such a “primary component” irradiates also the accretion disk, producing a “reflection component” in the X-ray spectrum. The illumination of the

<sup>1</sup>The other popular approach currently available to get information on the metric around BH candidates is the continuum-fitting method [12–14], i.e., the analysis of the disk’s thermal spectrum. The continuum-fitting method can be applied only to stellar-mass objects: the disk’s temperature scales as  $M^{-0.25}$  and for supermassive BH candidates the spectrum falls in the UV range, where dust absorption makes accurate measurements impossible.

\*bambi@fudan.edu.cn

cold disk by the primary component also produces spectral lines by fluorescence. The strongest line is the  $K\alpha$  iron line at 6.4 keV. Especially for some sources, this line is extraordinarily stable, in spite of a substantial variability of the continuum. This fact suggests that its shape is determined by the geometry of the spacetime around the compact object.

The profile of the  $K\alpha$  iron line depends on the background metric, the geometry of the emitting region, the disk emissivity, and the disk's inclination angle with respect to the line of sight of the distant observer. In the Kerr spacetime, the only relevant parameter of the background geometry is the spin  $a_* = J/M^2$ , while  $M$  sets the length of the system, without affecting the shape of the line. In those sources for which there is indication that the line is mainly emitted close to the compact object, the emission region may be thought to range from the radius of the innermost stable circular orbit (ISCO),  $r_{\text{in}} = r_{\text{ISCO}}$ , to some outer radius  $r_{\text{out}}$ . However, even more complicated geometries are possible. In principle, the disk emissivity could be theoretically calculated. In practice, that is not feasible at present. The simplest choice is an intensity profile  $I_e \propto r^\alpha$  with index  $\alpha < 0$  to be determined during the fitting procedure. The fourth parameter is the inclination of the disk with respect to the line of sight of the distant observer,  $i$ . The dependence of the line profile on  $a_*$ ,  $i$ ,  $\alpha$ , and  $r_{\text{out}}$  in the Kerr background has been analyzed in detail by many authors, starting with Ref. [15]. The case of deviations from the Kerr geometry is discussed in Ref. [17].

Roughly speaking, the calculation of the profile of the  $K\alpha$  iron line goes as follows. We want to compute the photon flux number density measured by a distant observer, which is given by

$$N_{E_{\text{obs}}} = \frac{1}{E_{\text{obs}}} \int I_{\text{obs}}(E_{\text{obs}}) d\Omega_{\text{obs}} = \frac{1}{E_{\text{obs}}} \int g^3 I_e(E_e) d\Omega_{\text{obs}}. \quad (1)$$

$I_{\text{obs}}$  and  $E_{\text{obs}}$  are, respectively, the specific intensity of the radiation and the photon energy as measured by the distant observer,  $d\Omega_{\text{obs}}$  is the element of the solid angle subtended by the image of the disk on the observer's sky,  $I_e$  and  $E_e$  are, respectively, the local specific intensity of the radiation and the photon energy in the rest frame of the emitter, and  $g = E_{\text{obs}}/E_e$  is the redshift factor.  $I_{\text{obs}} = g^3 I_e$  follows from the Liouville's theorem. As the  $K\alpha$  iron line is intrinsically narrow in frequency, we can assume that the disk emission is monochromatic (the rest frame energy is  $E_{K\alpha} = 6.4$  keV) and isotropic with a power-law radial profile:

$$I_e(E_e) \propto \delta(E_e - E_{K\alpha}) r^\alpha. \quad (2)$$

Doppler boosting, gravitational redshift, and frame dragging are encoded in the calculation of  $g$ , while the light bending enters in the integration. More details can be found in Ref. [17].

The purpose of this paper is to study how the  $K\alpha$  iron line observed in the X-ray spectrum of some supermassive

BH candidates in galactic nuclei can test the wormhole nature of these objects. A large number of wormhole spacetimes have been proposed in the literature [8]. Here, we restrict our attention to traversable wormholes with the line element given by [10,18]

$$ds^2 = -e^{2\Phi} dt^2 + \frac{dr^2}{1-b} + r^2[d\theta^2 + \sin^2\theta(d\phi - \omega dt)^2], \quad (3)$$

where  $\Phi$  and  $b$  are, respectively, the redshift and the shape function,<sup>2</sup> which, in the general case, may depend on both  $r$  and  $\theta$ .  $\omega$  determines the wormhole angular momentum. In what follows, we will assume  $\Phi = -r_0/r$  and  $\omega = 2J/r^3$ , where  $r_0$  is the throat radius and sets the scales of the system, just like the gravitational radius  $r_g = M$  does the same for the Kerr background.  $J$  is the wormhole spin angular momentum. The shape function considered in this work has the following form:

$$b = \left(\frac{r_0}{r}\right)^\gamma, \quad (4)$$

where  $\gamma$  is a constant.

The profile of the  $K\alpha$  iron line produced in the accretion disk around wormholes with  $\gamma = 1$  and different values of  $a_* = J/r_0^2$  is reported in the left panel of Fig. 1. The choice of the value of  $\gamma$ , and more in general of the form of  $g_{rr}$ , changes only the calculation of the photon trajectories, and therefore the effect of light bending, without altering the redshift factor  $g$ . The astrophysical parameters are  $i = 45^\circ$ ,  $\alpha = -3$ , and  $r_{\text{out}} = r_{\text{ISCO}} + 100r_0$ . For the reader familiar with the profile of the  $K\alpha$  iron line produced around Kerr BHs, it is straightforward to realize that the line of non-rotating and very slow-rotating wormholes looks similar to the one of mid- or fast-rotating Kerr BHs (see e.g., Fig. 1 in Ref. [17]). The line of wormholes with slightly higher spin has instead a peculiar low energy bump/peak, absent in the Kerr case. Such a peak moves to higher energies as the wormhole spin increases. The basic properties of the lines in these wormhole spacetimes and the differences with the Kerr ones can be understood in terms of ISCO radius and angular velocity of equatorial circular orbits.

As already discussed in Ref. [10], in these spacetimes  $r_{\text{ISCO}} = 2r_0$  for  $a_* = 0$  and decreases regularly to  $r_{\text{ISCO}} = 1.29r_0$  for  $a_* = 0.016693$ . For higher values of the spin, equatorial circular orbits are always stable, and therefore the inner radius of the disk is at  $r_0$ . This behavior should be compared with the one around a Kerr BH, noting that  $r_0$  plays the role of  $M$ . In Kerr,  $r_{\text{ISCO}} = 6M$  for  $a_* = 0$  and decreases regularly as the spin parameter increases, till  $r_{\text{ISCO}} = M$  for  $a_* = 1$ . For instance,  $r_{\text{ISCO}} = 2M$  when  $a_* \approx 0.943$ . This explains the low energy tail in the wormhole line: even for nonrotating or very slow-rotating

<sup>2</sup>The reader should note that the shape function is sometimes defined in a different way in the literature of wormholes.

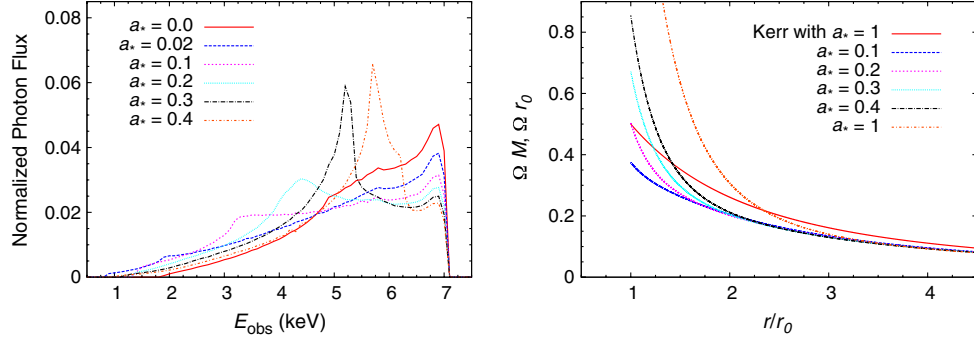


FIG. 1 (color online). Left panel: Broad  $K\alpha$  iron line in wormhole backgrounds with  $\gamma = 1$  and different values of the spin parameter  $a_*$ . The astrophysical parameters are viewing angle  $i = 45^\circ$ , intensity profile with index  $\alpha = -3$ , and emissivity region with inner radius  $r_{\text{in}} = r_{\text{ISCO}}$  and outer radius  $r_{\text{out}} = r_{\text{ISCO}} + 100r_0$ . Right panel: Angular frequency of equatorial circular orbits as a function of the radial coordinate  $r$  for the wormhole spacetimes with  $\gamma = 1$  and  $a_* = 0.1, 0.2, 0.3, 0.4$ , and 1, and the Kerr background with  $a_* = 1$ . See the text for details.

wormholes, the inner edge of the disk is at very small radii and therefore the line is affected by a strong gravitational redshift.

The low energy bump in the wormhole line, which becomes a pronounced peak when  $a_* \geq 0.2$ , is also generated at very small radii. This can be easily checked by calculating the contribution of the photons emitted at small radii; see Fig. 2. The high Doppler boosting is a consequence of the quick increase of the Keplerian angular velocity  $\Omega$ . The right panel of Fig. 1 shows  $\Omega$  for a Kerr BH with spin  $a_* = 1$  and for some traversable wormholes. For low and mid values of  $a_*$ , at radii  $r > 2r_0$  the angular velocity in wormhole spacetimes is quite independent of the wormhole spin and it is lower than the Kerr one. In such spacetimes, the wormhole spin plays an important role when  $r < 2r_0$ , and  $\Omega$  increases quickly as the radius decreases. The angular velocity can exceed the maximum angular velocity of the Kerr background  $\Omega_{\text{Kerr,max}} = 1/(2M)$ . The peak moves to higher energy as the wormhole spin increases, as the angular velocity at small radii also increases. If the value of the wormhole spin is high (e.g.,  $a_* = 1$ ), the peak produced by the Doppler boosting at small radii may be confused with the one of a Kerr BH produced at larger radii (see the right

panel in Fig. 2). However, in this case the wormhole line presents also a high energy tails, completely absent when the compact object is a Kerr BH.

If we change the value of the parameter  $\gamma$  in Eq. (4), we only affect the propagation of the photons from the disk to the observer, without altering the redshift factor, which does not depend on  $g_{rr}$ . Figure 3 shows the expected  $K\alpha$  iron line for traversable wormholes with  $\gamma = 2$  (left panel) and  $1/2$  (right panel). The qualitative properties of the line are the same of the case  $\gamma = 1$ . The line produced around nonrotating or very slow-rotating wormholes has the low energy tail similar to one expected from mid- or fast-rotating Kerr BHs. For slightly larger values of  $a_*$ , the line presents the low energy peak due to the gravitational redshift and Doppler blueshift at small radii. The limiting cases of very large and very small  $\gamma$  can be understood from the panels in Fig. 4. The left panel shows the case  $\gamma = 100$  and it is qualitatively very similar to the previous ones. Indeed, here the propagation of the photon is altered only in a very small region close to the wormhole throat ( $r_0/r$  is always smaller than 1). The right panel in Fig. 4 shows the opposite case, of very small  $\gamma$ , specifically with  $\gamma = 1/100$ . Now the propagation of photons is altered even at large radii

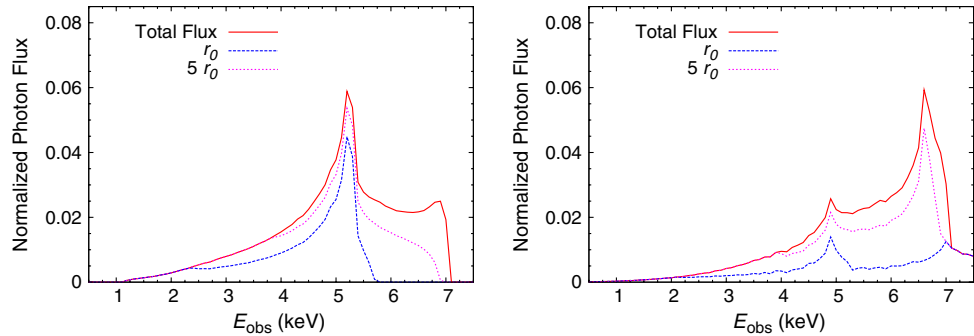


FIG. 2 (color online).  $K\alpha$  iron line in wormhole backgrounds with  $\gamma = 1$ ,  $a_* = 0.3$  (left panel) and 1 (right panel), viewing angle  $i = 45^\circ$ , intensity profile with index  $\alpha = -3$ , and emissivity region with inner radius  $r_{\text{in}} = r_{\text{ISCO}}$  and outer radius  $r_{\text{out}} = r_{\text{ISCO}} + 100r_0$ . The blue dashed line shows the contribution of the photon emitted in the region of the disk from the inner radius to  $r_{\text{ISCO}} + r_0$ . The magenta dotted line shows the one from the inner radius to  $r_{\text{ISCO}} + 5r_0$ .

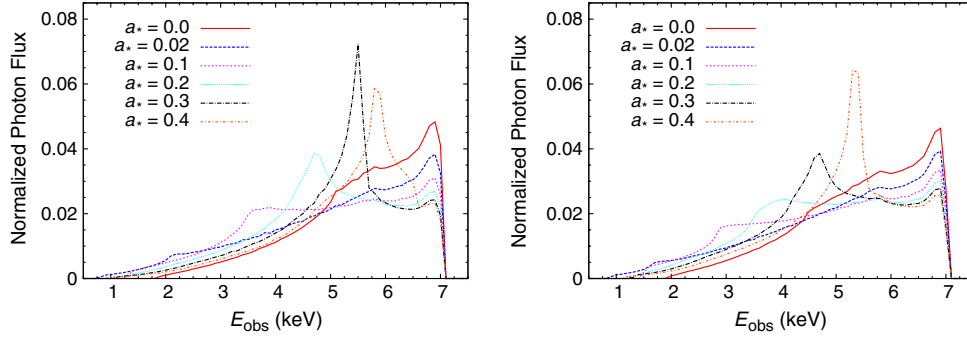


FIG. 3 (color online). Broad  $K\alpha$  iron line in wormhole backgrounds with  $\gamma = 2$  (left panel) and  $\gamma = 1/2$  (right panel) for different values of the spin  $a_*$ . The astrophysical parameters are viewing angle  $i = 45^\circ$ , intensity profile with index  $\alpha = -3$ , and emissivity region with inner radius  $r_{\text{in}} = r_{\text{ISCO}}$  and outer radius  $r_{\text{out}} = r_{\text{ISCO}} + 100r_0$ . See the text for details.

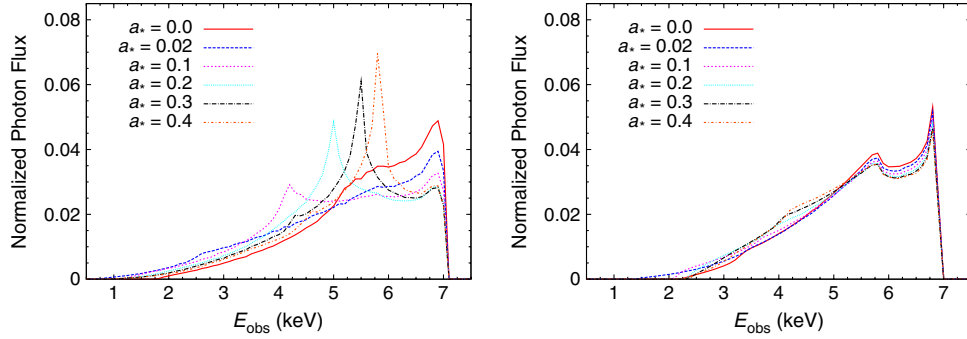


FIG. 4 (color online). Broad  $K\alpha$  iron line in wormhole backgrounds with  $\gamma = 100$  (left panel) and  $\gamma = 1/100$  (right panel) for different values of the spin  $a_*$ . The astrophysical parameters are viewing angle  $i = 45^\circ$ , intensity profile with index  $\alpha = -3$ , and emissivity region with inner radius  $r_{\text{in}} = r_{\text{ISCO}}$  and outer radius  $r_{\text{out}} = r_{\text{ISCO}} + 100r_0$ . See the text for details.

and the final effect is to significantly change the low energy peak, which becomes a small bump around 4 keV, quite independently of the value of the spin (the two peaks at  $\sim 6$  keV and  $\sim 7$  keV are instead the result, respectively, of the Doppler redshift and blueshift at larger radii).

### III. DISCUSSION

The analysis of the  $K\alpha$  iron line is commonly used to estimate the spin parameter of a BH candidate, under the assumption that the geometry of the spacetime around the object is described by the Kerr solution. The measurements reported in the literature of the supermassive BH candidates are shown in Table I. Roughly speaking, there are three objects that seem to be very fast-rotating Kerr BHs ( $a_* > 0.98$ ), and five objects that are consistent with Kerr BHs with a mid value of the spin parameter ( $a_* \sim 0.6$ – $0.8$ ).

What happens if the supermassive BH candidates are wormholes but we assume they are Kerr BHs and we try to estimate their spin parameter? Can a wormhole be confused with a Kerr BH of different spin? A qualitative answer to these questions has been already provided in the discussion in the previous section, but here we want to be more quantitative. We can compare the expected  $K\alpha$  iron line from a wormhole spacetime with the ones from

Kerr BHs. We use the same approach of Ref. [17] and we define the reduced  $\chi^2$  as

$$\chi_{\text{red}}^2(a_*, i, \alpha, r_{\text{out}}) = \frac{\chi^2}{n} = \frac{1}{n} \sum_{i=1}^n \frac{[N_i^{\text{Kerr}}(a_*, i, \alpha, r_{\text{out}}) - N_i^{\text{WH}}(\tilde{a}_*, \tilde{i}, \tilde{\alpha}, \tilde{r}_{\text{out}})]^2}{\sigma_i^2}, \quad (5)$$

where the summation is performed over  $n$  sampling energies  $E_i$  and  $N_i^{\text{Kerr}}$  and  $N_i^{\text{WH}}$  are the normalized photon fluxes in the energy bin  $[E_i, E_i + \Delta E]$  respectively for

TABLE I. Current measurements of the spin parameter of supermassive BH candidates with the analysis of the  $K\alpha$  iron line.

AGN	$a_*$	References
MGC-6-30-15	$>0.98$	[19]
Fairall 9	$0.65 \pm 0.05$	[20,21]
SWIFT J2127.4 + 5654	$0.6 \pm 0.2$	[22]
1H 0707-495	$>0.98$	[23]
Mrk 79	$0.7 \pm 0.1$	[24]
NGC 3783	$>0.98$	[25]
Mrk 335	$0.70 \pm 0.12$	[21]
NGC 7469	$0.69 \pm 0.09$	[21]

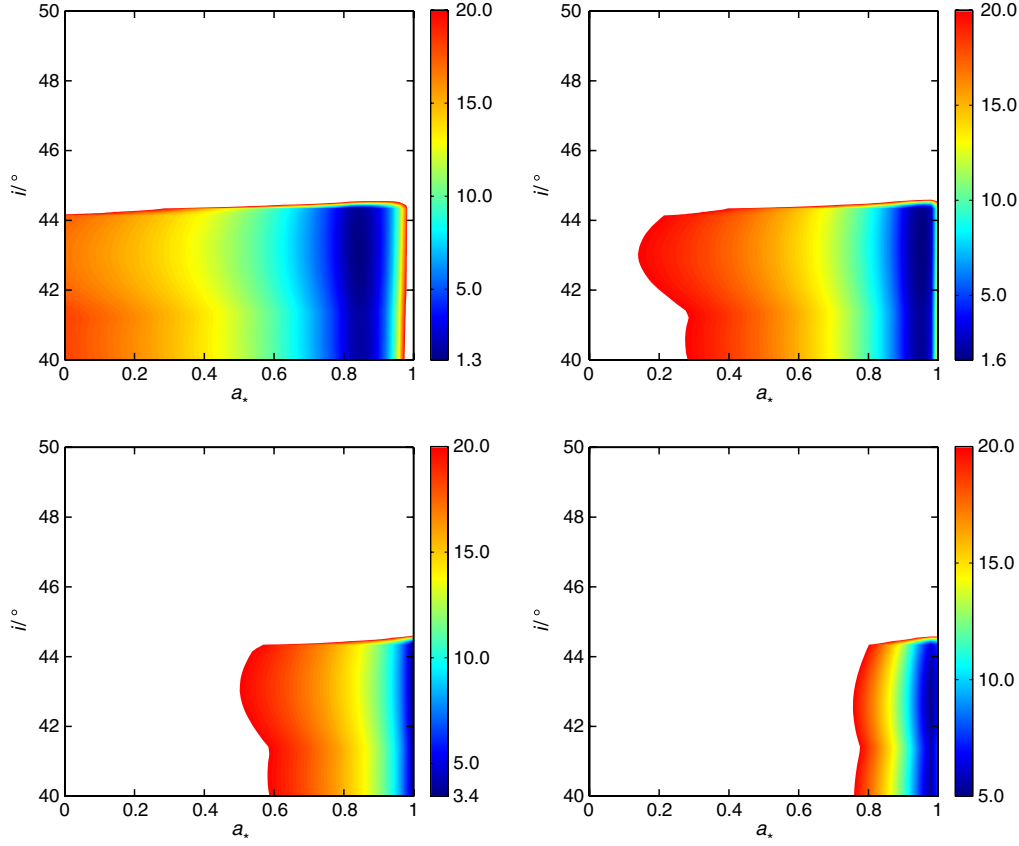


FIG. 5 (color online). Reduced  $\chi^2$  from the comparison of the profile of the  $K\alpha$  iron line produced in a Kerr spacetime with spin parameter  $a_*$  and observed with a viewing angle  $i$  and the line generated in a wormhole background with  $\gamma = 1$ , spin parameter  $\tilde{a}_* = 0$  (top left panel), 0.015 (top right panel), 0.02 (bottom left panel), and 0.3 (bottom right panel), and observed with a viewing angle  $\tilde{i} = 45^\circ$ . The intensity profile has index  $\alpha = \tilde{\alpha} = -3$  and the emissivity region has an inner radius at the ISCO and  $r_{\text{out}} - r_{\text{ISCO}} = \tilde{r}_{\text{out}} - \tilde{r}_{\text{ISCO}} = 100r_0$ . See the text for details.

the Kerr and the wormhole metric. Here the error  $\sigma_i$  is assumed to be 15% the normalized photon flux  $N_i^{\text{WH}}$ ,

$$\sigma_i = 0.15N_i^{\text{WH}}, \quad (6)$$

which is roughly the accuracy of current observations in the best situations. For the calculation of  $N_i^{\text{Kerr}}$ , we use the general form of the Kerr metric

$$ds^2 = \left(1 - \frac{2mr}{\Sigma}\right)dt^2 + \frac{4amr\sin^2\theta}{\Sigma}dt d\phi - \frac{\Sigma}{\Delta}dr^2 - \Sigma d\theta^2 - \sin^2\theta \left(r^2 + a^2 + \frac{2a^2mr\sin^2\theta}{\Sigma}\right)d\phi^2, \quad (7)$$

where  $a = J/M$ ,  $\Sigma = r^2 + a^2\cos^2\theta$ , and  $\Delta = r^2 - 2mr + a^2$ , so both Eqs. (3) and (7) are valid for arbitrary values of the spin parameter (but for the Kerr metric it makes sense to consider only the case  $|a_*| \leq 1$ ).

Let us start considering a wormhole background with  $\gamma = 1$ . In this simplified analysis, we assume  $\alpha = \tilde{\alpha}$  and  $r_{\text{out}} = \tilde{r}_{\text{out}}$ . The reduced  $\chi^2$  for wormholes with spin parameter  $\tilde{a}_* = 0, 0.015, 0.02$ , and 0.3 and viewing angle  $\tilde{i} = 45^\circ$  is shown in Fig. 5. The values of  $a_*$  and  $i$  at the

minimum of the reduced  $\chi^2$  are reported in Table II. The minimum of  $\chi_{\text{red}}^2$  is at a viewing angle  $i$  slightly lower than  $\tilde{i}$  because the wormhole angular frequency at large radii is lower than the Kerr one and the high energy peak of the line is produced by the Doppler blueshift at relatively large

TABLE II. Minimum of the reduced  $\chi^2$  and the corresponding Kerr values of  $a_*$  and  $i$  for the lines produced by wormholes with  $\gamma$  and  $\tilde{a}_*$  given in the first and second column, and  $\tilde{i} = 45^\circ$ . See the text for more details.

$\gamma$	$\tilde{a}_*$	$\chi_{\text{red,min}}^2$	$a_*$	$i$
1	0	1.31	0.84	43.2°
1	0.015	1.62	0.96	43.4°
1	0.02	3.43	1	43.2°
1	0.3	5.69	0.98	42.6°
2	0	0.90	0.84	43.2°
2	0.02	2.87	1	43.2°
1/2	0	2.06	0.84	42.4°
1/2	0.02	2.79	1	42.8°
1/100	0	2.27	0.72	40.0°
1/100	0.4	5.64	0.70	40.0°

radii. For nonrotating or very slow-rotating wormholes ( $\tilde{a}_* = 0$  and  $0.015$ ), the minimum of  $\chi_{\text{red}}^2$  is around 1, which means that these lines may well fit the ones expected for a Kerr BH, providing, however, a completely wrong estimate of the spin  $a_*$ . Indeed,  $a_*$  is in the range  $0.84$ – $1$ . Such a value of the spin parameter is marginally consistent with the current measurements shown in Table I. For  $a_* = 0.02$ , the fit is already quite bad, as the minimum of  $\chi_{\text{red}}^2$  is  $\sim 3$  (bottom left panel in Fig. 5). As the wormhole spin increases, the fit becomes worse and worse. If  $\tilde{a}_* = 0.3$ , the minimum of  $\chi_{\text{red}}^2$  is  $\sim 5$  (bottom right panel in Fig. 5). For high values of the wormhole spin, e.g.,  $a_* = 1$ , the peak produced by Doppler boosting at small radii may look like the one of a Kerr BH. However, as already pointed out in the previous section, there is now a high energy tail absent in the Kerr line. The fit is therefore bad: for instance, if  $a_* = 1$ , the minimum of  $\chi_{\text{red}}^2$  is  $\sim 8$ . While a rigorous analysis would require us to consider real data of specific sources, the fact that current X-ray data give good fits when the Kerr metric is assumed and that already for  $a_* \gtrsim 0.02$  we find  $\chi_{\text{red,min}}^2 > 3$  can be used to conclude that rotating wormholes with a moderate value of the spin parameter may already be ruled out as candidates

to explain the supermassive objects at the centers of galaxies.

For a different value of  $\gamma$ , the situation is similar (except for very small values of  $\gamma$ ), as shown in Figs. 6 and 7. Nonrotating wormholes with higher values of  $\gamma$  seem to produce spectra more similar to the one expected from Kerr BHs. When  $\gamma$  is very small, one finds contour plots like the ones in Fig. 8 (some caution in the interpretation of these plots is necessary here, as  $\chi_{\text{red,min}}^2$  is for  $i < 40^\circ$ , but from the contour plots of the previous cases, it is straightforward to guess the behavior for lower angles). Despite the quite different line for very low values of  $\gamma$ , for nonrotating wormholes we still find marginally acceptable fits, while for rotating wormholes the fits are bad.

As a final remark, we can note that the  $K\alpha$  iron line analysis can also be used to test the nature of stellar-mass BH candidates and verify if they are Kerr BHs or traversable wormholes, even if the possibility of the existence of stellar-mass traversable wormholes seems to be less theoretically motivated. The iron line approach cannot instead be used to probe the geometry of the spacetime around stellar-type compact objects like neutron stars, as in this case the inner edge of the accretion disk is determined by

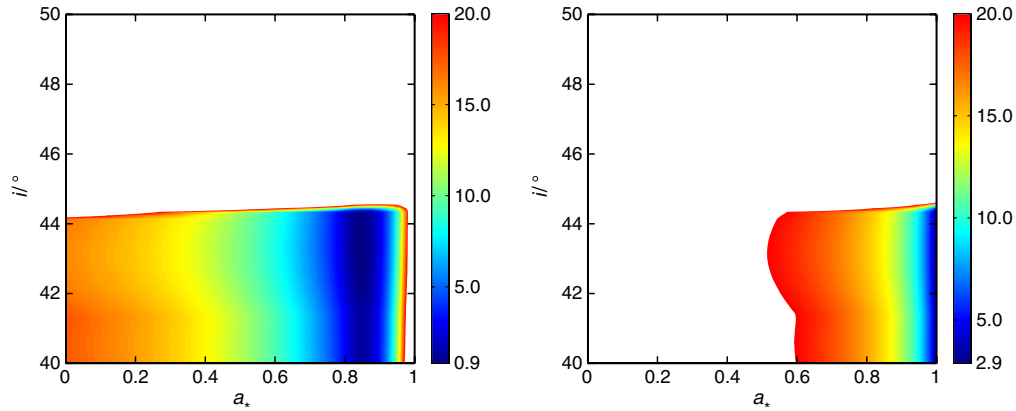


FIG. 6 (color online). As in Fig. 5, for the case  $\gamma = 2$ . The spin parameters are  $\tilde{a}_* = 0$  (left panel) and  $0.02$  (right panel).

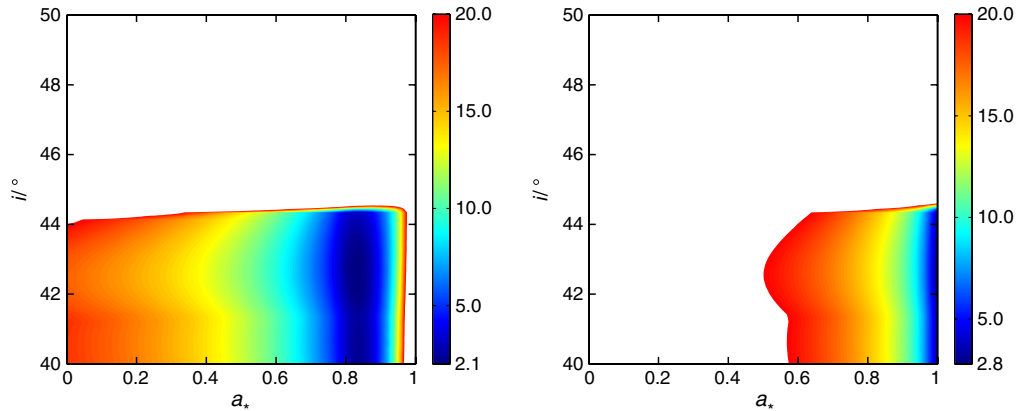


FIG. 7 (color online). As in Fig. 5, for the case  $\gamma = 1/2$ . The spin parameters are  $\tilde{a}_* = 0$  (left panel) and  $0.02$  (right panel).

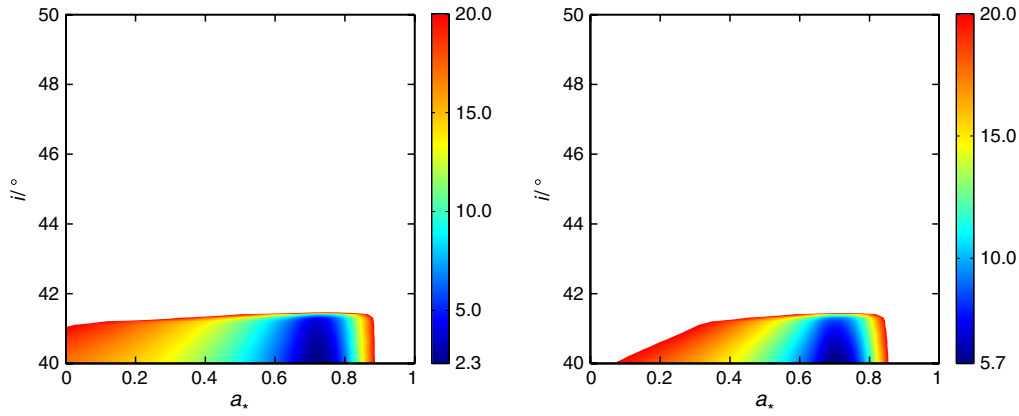


FIG. 8 (color online). As in Fig. 5, for the case  $\gamma = 1/100$ . The spin parameter is  $\tilde{a}_* = 0$  (left panel) and 0.4 (right panel).

the magnetosphere, rather than by the background metric, and it is at larger radii.

#### IV. SUMMARY AND CONCLUSIONS

It has been proposed that the supermassive objects at the centers of galaxies may be wormholes formed in the early Universe and connecting either our Universe with other universes, or two different regions of our Universe. The wormhole paradigm may explain the observations of very massive objects already at high redshift, as well as the non-observation of thermal radiation from the putative surface of these objects. In this paper, we have investigated how the analysis of the profile of the  $K\alpha$  iron line can test the wormhole nature of the supermassive BH candidates. While observational tests to distinguish wormholes from Kerr BHs have already been discussed by other authors, the  $K\alpha$  iron line approach has never been considered so far, despite the fact that it is currently the only available technique to probe the spacetime geometry around these objects.

The traversable wormholes discussed in this paper have the line element given in Eq. (3). Their most important feature is that the ISCO radius is close to the wormhole throat already in the nonrotating case. The radiation emitted in the inner part of the accretion disk is thus strongly redshifted. This leads to a low energy tail in the line seen by a distant observer similar to the one of a Kerr BH with a mid or high value of  $a_*$ . Already for very moderate values of the wormhole spin parameter, the angular velocity of

equatorial circular orbits increases quickly at small radii, producing a low energy peak in the observed line. Such a feature is not present in the case of Kerr BHs and thus represents an important observational signature of rotating wormholes. However, a similar feature has never been observed in the X-ray spectrum of BH candidates. A more quantitative analysis of the comparison of the line expected from a wormhole with the one expected from a Kerr BH confirms this picture; see Figs. 5–8. Nonrotating or very slow-rotating wormholes may be confused with mid- or fast-rotating Kerr BHs by current observations (but with future more accurate observations we should be able to distinguish the two cases). The wormholes with slightly higher value of the spin parameter are distinguishable from Kerr BHs by current observations and they may already be ruled out. This conclusion is based on the fact that current analysis of the  $K\alpha$  iron lines of some supermassive BH candidates produce good fits ( $\chi^2_{\text{red,min}} \sim 1$ ) when the Kerr background is assumed [19–25]. The study presented in this work does not exclude all the rotating wormholes, but only the one with the line element given by Eq. (3). For instance, for wormholes traversable in only one direction, the outside geometry may be the same as the one of Kerr BHs [26].

#### ACKNOWLEDGMENTS

I thank Zilong Li for help in the preparation of the manuscript. This work was supported by the Thousand Young Talents Program and Fudan University.

- 
- [1] J. Kormendy and D. Richstone, *Annu. Rev. Astron. Astrophys.* **33**, 581 (1995).
  - [2] C. Bambi, *Mod. Phys. Lett. A* **26**, 2453 (2011); *Astron. Rev.* **8**, 4 (2013).
  - [3] C. Bambi and K. Freese, *Phys. Rev. D* **79**, 043002 (2009); C. Bambi and N. Yoshida, *Classical Quantum Gravity* **27**,

- 205006 (2010); C. Bambi, *Phys. Rev. D* **83**, 103003 (2011); *Phys. Lett. B* **705**, 5 (2011); C. Bambi, F. Caravelli, and L. Modesto, *Phys. Lett. B* **711**, 10 (2012); C. Bambi, *Phys. Rev. D* **85**, 043001 (2012); Z. Li and C. Bambi, *J. Cosmol. Astropart. Phys.* **03** (2013) 031; C. Bambi and G. Lukes-Gerakopoulos, *arXiv:1302.0565*.

- [4] E. Maoz, *Astrophys. J.* **494**, L181 (1998).
- [5] A. E. Broderick, A. Loeb, and R. Narayan, *Astrophys. J.* **701**, 1357 (2009).
- [6] M. A. Abramowicz, W. Kluzniak, and J.-P. Lasota, *Astron. Astrophys.* **396**, L31 (2002); C. Bambi, [arXiv:1205.4640](#).
- [7] X. Fan *et al.* (SDSS Collaboration), *Astron. J.* **122**, 2833 (2001); D. J. Mortlock, S. J. Warren, B. P. Venemans, M. Patel, P. C. Hewett, R. G. McMahon, C. Simpson, T. Theuns *et al.*, *Nature (London)* **474**, 616 (2011).
- [8] M. Visser, *Lorentzian Wormholes: From Einstein to Hawking* (Springer-Verlag, New York, 2002); N. S. Kardashev, I. D. Novikov, and A. A. Shatskiy, *Int. J. Mod. Phys. D* **16**, 909 (2007).
- [9] J. G. Cramer, R. L. Forward, M. S. Morris, M. Visser, G. Benford, and G. A. Landis, *Phys. Rev. D* **51**, 3117 (1995); T. Harko, Z. Kovacs, and F. S. N. Lobo, *Phys. Rev. D* **78**, 084005 (2008); F. Abe, *Astrophys. J.* **725**, 787 (2010); Y. Toki, T. Kitamura, H. Asada, and F. Abe, *Astrophys. J.* **740**, 121 (2011); N. Tsukamoto, T. Harada, and K. Yajima, *Phys. Rev. D* **86**, 104062 (2012); C.-M. Yoo, T. Harada, and N. Tsukamoto, [arXiv:1302.7170](#)
- [10] T. Harko, Z. Kovacs, and F. S. N. Lobo, *Phys. Rev. D* **79**, 064001 (2009).
- [11] A. C. Fabian, K. Iwasawa, C. S. Reynolds, and A. J. Young, *Publ. Astron. Soc. Pac.* **112**, 1145 (2000); C. S. Reynolds and M. A. Nowak, *Phys. Rep.* **377**, 389 (2003).
- [12] L.-X. Li, E. R. Zimmerman, R. Narayan, and J. E. McClintock, *Astrophys. J. Suppl. Ser.* **157**, 335 (2005); J. E. McClintock, R. Narayan, S. W. Davis, L. Gou, A. Kulkarni, J. A. Orosz, R. F. Penna, R. A. Remillard, and J. F. Steiner, *Classical Quantum Gravity* **28**, 114009 (2011).
- [13] C. Bambi and E. Barausse, *Astrophys. J.* **731**, 121 (2011); C. Bambi, *Astrophys. J.* **761**, 174 (2012).
- [14] C. Bambi, *Phys. Rev. D* **85**, 043002 (2012); **86**, 123013 (2012).
- [15] A. C. Fabian, M. J. Rees, L. Stella, and N. E. White, *Mon. Not. R. Astron. Soc.* **238**, 729 (1989).
- [16] Y. Tanaka, K. Nandra, A. C. Fabian, H. Inoue, C. Otani, T. Dotani, K. Hayashida, K. Iwasawa *et al.*, *Nature (London)* **375**, 659 (1995).
- [17] C. Bambi, *Phys. Rev. D* **87**, 023007 (2013).
- [18] E. Teo, *Phys. Rev. D* **58**, 024014 (1998).
- [19] L. W. Brenneman and C. S. Reynolds, *Astrophys. J.* **652**, 1028 (2006).
- [20] S. Schmoll, J. M. Miller, M. Volonteri, E. Cackett, C. S. Reynolds, A. C. Fabian, L. W. Brenneman, G. Miniutti, and L. C. Gallo, *Astrophys. J.* **703**, 2171 (2009).
- [21] A. R. Patrick, J. N. Reeves, D. Porquet, A. G. Markowitz, A. P. Lobban, and Y. Terashima, *Mon. Not. R. Astron. Soc.* **411**, 2353 (2011).
- [22] G. Miniutti, F. Panessa, A. De Rosa, A. C. Fabian, A. Malizia, M. Molina, J. M. Miller, and S. Vaughan, *Mon. Not. R. Astron. Soc.* **398**, 255 (2009).
- [23] A. C. Fabian, A. Zoghbi, R. R. Ross, P. Uttley, L. C. Gallo, W. N. Brandt, A. Blustin, T. Boller *et al.*, *Nature (London)* **459**, 540 (2009).
- [24] L. C. Gallo, G. Miniutti, J. M. Miller, L. W. Brenneman, A. C. Fabian, M. Guainazzi, and C. S. Reynolds, *Mon. Not. R. Astron. Soc.* **411**, 607 (2011).
- [25] L. W. Brenneman, C. S. Reynolds, M. A. Nowak, R. C. Reis, M. Trippe, A. C. Fabian, K. Iwasawa, J. C. Lee *et al.*, *Astrophys. J.* **736**, 103 (2011).
- [26] N. J. Poplawski, *Phys. Lett. B* **687**, 110 (2010).